FEBS Letters 584 (2010) 878–882

FEBS Letters

journal homepage: www.FEBSLetters.org

Crystal structure of the LMAN1-CRD/MCFD2 transport receptor complex provides insight into combined deficiency of factor V and factor VIII

Edvard Wigren, Jean-Marie Bourhis [1], Inari Kursula [2], Jodie E. Guy, Ylva Lindqvist *

Dept. of Medical Biochemistry and Biophysics, Karolinska Institutet, 17177 Stockholm, Sweden

ARTICLE INFO

Article history:
Received 12 January 2010
Revised 29 January 2010
Accepted 1 February 2010
Available online 9 February 2010

Edited by Kaspar Locher

Keywords:
Glycoprotein transport
ER quality control
Protein complex
Crystal structure
ERGIC-53

ABSTRACT

LMAN1 is a glycoprotein receptor, mediating transfer from the ER to the ER–Golgi intermediate compartment. Together with the co-receptor MCFD2, it transports coagulation factors V and VIII. Mutations in LMAN1 and MCFD2 can cause combined deficiency of factors V and VIII (F5F8D). We present the crystal structure of the LMAN1/MCFD2 complex and relate it to patient mutations. Circular dichroism data show that the majority of the substitution mutations give rise to a disordered or severely destabilized MCFD2 protein. The few stable mutation variants are found in the binding surface of the complex leading to impaired LMAN1 binding and F5F8D.

Structured summary:
MINT-7557086: *lman1* (uniprotkb:P49257) and *mcfd2* (uniprotkb:Q8NI22) *bind* (MI:0407) by *X-ray crystallography* (MI:0114)

1. Introduction

Combined deficiency of coagulation factors V and VIII (F5F8D) is an autosomal recessive bleeding disorder, with plasma levels of coagulation factors FV and FVIII reduced to 5–30% of normal levels [1,2]. This is due to mutations in the genes coding for either LMAN1 (lectin mannose-binding protein 1, also known as ERGIC-53) [3] or MCFD2 (multiple coagulation factor deficiency 2) [4]. FVIII interacts with the LMAN1/MCFD2 complex, while the B-domain deleted form of FVIII exhibits reduced binding [5]. LMAN1/MCFD2 complex formation and FVIII binding are calcium ion dependent [6–8].

LMAN1 protein was originally identified as a marker for the ER–Golgi intermediate compartment (ERGIC). From the link to F5F8D, LMAN1 was revealed to be a sorting receptor, mediating transport of certain glycoproteins from the ER to the ERGIC [8]. LMAN1 exists as homohexamers that cycle between the ER and the ERGIC [9], binding correctly folded glycosylated cargo proteins, including FV and FVIII, in the ER, recruiting the cargo for package into COPII (coat protein II) coated vesicles and transport to the ERGIC. Many proteins have been shown to act as cargo for LMAN1 besides FV and FVIII e.g. cathepsin Z and cathepsin C [8,10], α1-antitrypsin [11], and sulfatase modifying factor 1 [12].

LMAN1 is a type-1 transmembrane protein containing an ER translocation signal sequence, a lumenal, a transmembrane, and a short cytoplasmic domain. The lumenal domain can be divided into an N-terminal carbohydrate recognition domain (CRD) (residues 31–285) and a membrane-proximal stalk domain. The CRD is responsible for the calcium ion dependent binding of mannose-rich glycans. The stalk domain is thought to mediate oligomerization of LMAN1 [9], while the cytoplasmic tail contains a COPII binding and an ER retrieval motif. The crystal structures of the CRD, in apo- and Ca^{2+}-bound form [13,14] show similarity to Ca^{2+}-dependent leguminous lectins, confirming the role of LMAN1 as a glycoprotein receptor.

Mutations in *MCFD2* cause the same clinical phenotype as mutations in *LMAN1* [2,4]. MCFD2 is only known to be required for transport of FV and FVIII and may act as a specific recruitment factor for these LMAN1 cargo proteins. *MCFD2* encodes a highly conserved 16-kDa soluble protein, which does not include motifs for COPII binding or ER retrieval; correct localization of MCFD2 is reliant on its binding to LMAN1. NMR studies [7] have shown that MCFD2 is unfolded in the absence of Ca^{2+} ions and that Ca^{2+} binding induces folding of two C-terminal EF-hand motifs, explaining the Ca^{2+} ion dependence for formation of the LMAN1–MCFD2 complex.

Presently, 32 mutations in *LMAN1* [2,3,15] and 16 mutations in *MCFD2* leading to F5F8D have been identified [2,16,17]. To gain

* Corresponding author. Address: Dept. of Medical Biochemistry and Biophysics, Tomtebodavägen 6, Karolinska Institutet, S-17177 Stockholm, Sweden.
E-mail address: ylva.lindqvist@ki.se (Y. Lindqvist).
[1] Present address: IBCP UMR 5086 CNRS, 7, Passage du Vercors, 69367 Lyon cedex 07, France.
[2] Present address: Helmholtz Centre for Infection Research and University of Hamburg, CSSB-HZI at DESY, Notkestrasse 85, Bldg. 25b, 22607 Hamburg, Germany.

0014-5793/$36.00 © 2010 Federation of European Biochemical Societies. Published by Elsevier B.V. All rights reserved.
doi:10.1016/j.febslet.2010.02.009

insight into the interaction between LMAN1 and MCFD2, and further explain the consequences of mutations found in F5F8D patients we have determined the crystal structure of the complex between the CRD of LMAN1 and MCFD2 and have characterized F5F8D patient mutations.

2. Materials and methods

2.1. Cloning

The cDNAs corresponding to the two EF-hand motifs of human MCFD2 (residues 58–146) thus excluding the N-terminal unstructured region (MCFD2-N), and the CRD of human LMAN1 (residues 32–277) were amplified by PCR. The resulting fragments were cloned into the expression vector pET-28a (Novagen), with a thrombin cleavable 6× His-tag. An additional N-terminal GST-tag was inserted into the vector containing the CRD. Full-length MCFD2, excluding the signal sequence, was cloned as previously described [7]. Amino acid substitutions were introduced into full-length MCFD2 using the QuikChange site-directed mutagenesis kit (Stratagene).

2.2. Expression and purification

MCFD2 constructs and mutant variants were expressed in *Escherichia coli* and purified by Ni–NTA affinity chromatography as previously described [7]. LMAN1-CRD was expressed in *E. coli* at 16 °C for ~60 hours in auto-induction media [18]. The cells were harvested by centrifugation, re-suspended in lysis-buffer (50 mM Tris–HCl pH 8.5, 250 mM NaCl, 10 mM imidazole, 20 mM $CaCl_2$ and 0.05% w/v PMSF), and lysed by sonication at 4 °C. The proteins were purified by Ni–NTA affinity chromatography, followed by affinity purification using glutathione-Sepharose 4B resin (Pharmacia), and cleaved with thrombin to remove the GST-tag. After mixing LMAN1-CRD with MCFD2-N, the LMAN1-CRD/MCFD2-N complex was purified on a Superdex 75 column (GE Healthcare) in 50 mM Tris–HCl pH 8.5 containing 250 mM NaCl and 20 mM $CaCl_2$.

2.3. Crystallization, data collection and data processing

Crystals of a complex comprising the LMAN1-CRD and MCFD2-N were grown at 4 °C using the sitting drop method by mixing 1 μl of protein (6.5 mg/ml) with 0.5 μl of precipitation solution (20% PEG6000, 0.1 M ammonium chloride 0.1 M Hepes, pH 7). Crystals were flash frozen in liquid nitrogen using 30% glycerol as cryoprotectant. X-ray diffraction data were collected to 2.45 Å resolution at 100 K on beamline BM14 at the ESRF (Grenoble, France) using a wavelength of 0.9537 Å and 0.2° oscillation angle. The data was processed using XDS [19] and the CCP4-suite [20]. Table 1 shows statistics of the data.

2.4. Structure determination and refinement

Data reduction indicated the space group as P622 but further analysis showed that the data were merohedrally twinned with true space group $P6_1$. Initial phases were obtained by molecular replacement using the program Phaser [21], with the crystal structure of the CRD of rat LMAN1 (PDB code 1R1Z [14]) as search model. One clear solution in space group $P6_1$ with two subunits in the asymmetric unit was obtained. Attempts to position the MCFD2 subunits by molecular replacement with the NMR-model of MCFD2 [7] were unsuccessful. However, the initial molecular replacement electron density map of the CRD showed additional electron density where, after density modification with Parrot [22], two helices could be placed. Iterative model building in Coot [23] and refinement with Refmac5 [24] then allowed modelling of the two MCFD2 molecules. The twin refinement protocol implemented in Refmac5 was employed in addition to anisotropic scaling and simple bulk solvent correction. Tight NCS restraints were applied for both the CRD and MCFD2; releasing these restraints at the end did not lower the R_{free}-value. The coordinates and structure factors have been deposited in the Protein Databank with accession number 3LCP.

Table 1
Data collection and refinement.

Data collection	
Space group	$P6_1$
Unit cell	a = 56.6 Å, c = 396.9 Å
Resolution (Å)	2.45
Unique reflections	26465
Redundancy	11.8 (7.3)
R_{sym} (%)	12 (30)
I/σ	17.6 (5.8)
Completeness (%)	98.9 (85.6)
⟨B⟩ Wilson plot (Å^2)	43.0
Refinement	
Number of reflections	
Work set	25039 (1672)
Test set	1426 (87)
Number of atoms	
Protein	4695
Water	109
Ca^{2+} ions	8
R_{factor}	19.6 (26.1)
R_{free}	24.7 (40.5)
Average B-factors (Å^2)	
Protein (CRD)	23.6
Protein (MCFD2)	27.8
Ca^{2+} ions	28.9
Water molecules	23.4
Bond length R.M.S.D. (Å)	0.016
Bond angle R.M.S.D. (°)	1.47
Ramachandran plot	
Percentage in preferred regions	93.9
Percentage in additional allowed regions	5.2
Percentage in disallowed regions	0.8
Twin fraction	
h, k, l	0.732
$-h-k, k, -l$	0.268

Numbers in parenthesis refer to highest resolution shell (2.51–2.45 Å).

2.5. Circular dichroism spectroscopy

Circular dichroism (CD) measurements were conducted on a JASCO J-810 spectropolarimeter using a cuvette of 0.1 cm path length. All proteins were at a concentration of 0.1 mg/ml in 5 mM Bis–Tris buffer pH 7.4, with 5 mM $CaCl_2$. The spectra were recorded from 195 to 260 nm at 20 °C. Ten scans were averaged and corrected for the buffer spectrum. Thermal unfolding experiments were performed by monitoring the CD signal at 222 nm between 20 and 90 °C using a heating rate of 2 °C/min. Melting points (Tm) were calculated using sigmoidal fit in GraphPad Prism (GraphPad Software, Inc.).

3. Results

3.1. Structure

The structure of the complex of the CRD from LMAN1 and MCFD2-N was determined by molecular replacement from merohedrally twinned crystals to 2.45 Å resolution in space group $P6_1$ with two complexes in the asymmetric unit. The electron density map is continuous for the CRD from residue 41–274

(residue numbering include signal sequence), and with exceptions of a few solvent exposed side chains, all residues are well-defined. The MCFD2 molecule is less well ordered and only residues 66–98 and residues 110–144 have been modelled (residue numbers include the signal sequence). The overall quality of the model is as expected for this resolution and 94% of the residues are found in the most favoured region of the Ramachandran plot (Table 1). The structures of the two complexes in the asymmetric unit are identical within the error limits of the electron density map.

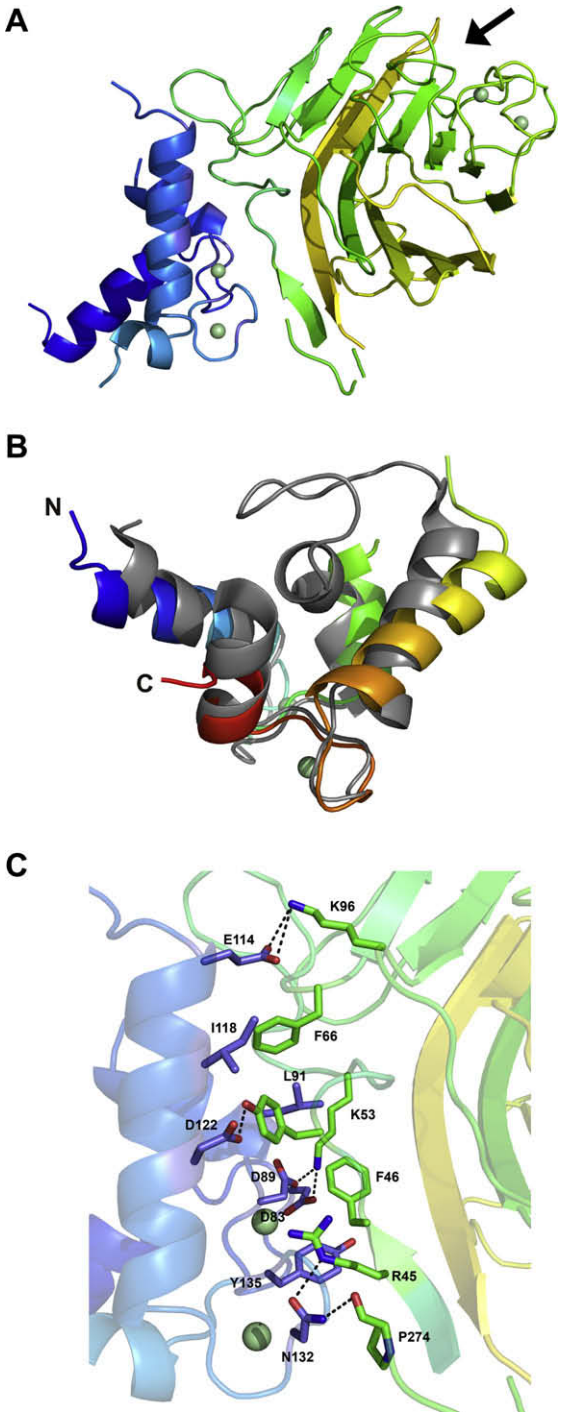

Fig. 1. (A) Structure of the complex. MCFD2 (blue) and the CRD (green). The presumed carbohydrate binding site on the CRD is indicated with an arrow. (B) Superposition of the MCFD2 structure determined by NMR (grey) and MCFD2 in the complex (rainbow coloured). (C) The interface between MCFD2 (blue) and the CRD (green). Interacting residues are labeled. Hydrogen bonds are shown as dashed lines. Figs. 1 and 2A was prepared with PyMol [25].

The CRD comprises two β-sheets packed into a β-sandwich (Fig. 1A), with two calcium ions bound in the presumed carbohydrate binding site on the concave face. Comparison of the human CRD in the complex with the structure of the free rat CRD protein [14] shows that the N-terminal residues corresponding to residues 25–44 in the rat protein are disordered in the complex due to binding of MCFD2 at that location. Both structures of the rat CRD indicated inherent flexibility in these residues. No other major structural perturbations in the CRD have occurred upon complex formation; and superposition of the two structures gives an R.M.S.D. of 0.32 Å for 227 Cα-atoms.

MCFD2 is composed of a flexible N-terminal region and two EF-hand calcium ion binding motifs. A comparison between the lowest energy structure of MCFD2 determined by NMR [7] and MCFD2 in the complex shows deviations (Fig. 1B); 59 Cα-atoms can be aligned with an R.M.S.D. of 2.3 Å. The NMR-analysis showed the protein to be inherently very dynamic, the N-terminal 43 residues of the mature protein could not be assigned to structure and the loop consisting of residues 101–109 is very flexible [7]. The first helix and Ca^{2+} binding loop are reasonably well aligned to the NMR-structure whereas in the complex the C-terminal part of the following bent helix is now straight. The flexible loop is not seen in the electron density. The last helix–Ca^{2+}-loop–helix motif is approximately aligned but the last turn of the terminal helix is not observed.

Binding of MCFD2 to the CRD buries a surface area of 850 $Å^2$, ~17% of the surface area of the ordered part of MCFD2. Six hydrogen bonds, three ionic interactions and a few water-mediated hydrogen bonds are formed upon complex formation. MCFD2 is bound to the CRD on the opposite side relative to the carbohydrate recognition site, close to the surface on the convex β-sheet suggested to constitute a binding area for the protein part of the glycoprotein cargo (Fig. 1A and C). The main interaction area on the CRD is made up of residues H43-F46, Y48-K49, S51-H56, Q59-D61 and T63-F66, which encompass the first ordered residues, the first β-strand in the convex sheet, which contains a turn of 3_{10}-helix structure in the middle, and the long loop that follows before β-strand 2. In MCFD2, several interacting residues are found in the first Ca^{2+}-binding loop and the proceeding helix. These include residues Y82 and D83, the latter is one of the Ca^{2+} ligands, and together with D89, makes salt bridges to K53 in the CRD. Other interacting residues are G90-E92, where E92 is another Ca^{2+} ligand in the first EF-hand which is hydrogen bonded to K53 via a water molecule, residues S94-T95, and T98-H99. In the first helix of the second EF-hand, residues L111, E114, I118, I121, D122 and L125 interact; E114 forms a salt bridge with K96 and D122 makes a hydrogen bond with the side chain of Y48 on the CRD. In the Ca^{2+} binding loop, the side chain of residue D129 forms a water mediated bond to the R45 side chain, the side chain of N132 forms hydrogen bonds with the carbonyl of P274 and the R45 side chain, the main chain carbonyl of D133 forms a hydrogen bond to the main chain nitrogen of F46, and G134 and Y135 pack against residue F46 in the CRD (Fig. 1C).

In the crystal, MCFD2 also makes contact with another symmetry-related CRD molecule, but this buries a smaller surface area of 590 $Å^2$, includes only two hydrogen bonds and one salt bridge, and is likely to be a crystallization artefact. A CRD/MCFD2 complex structure, determined from untwinned crystals in another space group just appeared in the Protein Data Bank (3A4U). Superposition shows the structures to be essentially the same, involving the same interactions between the CRD and MCFD2.

3.2. CD measurements

It has been shown that the structural integrity of MCFD2 relies on the ability to bind calcium and formation of a small

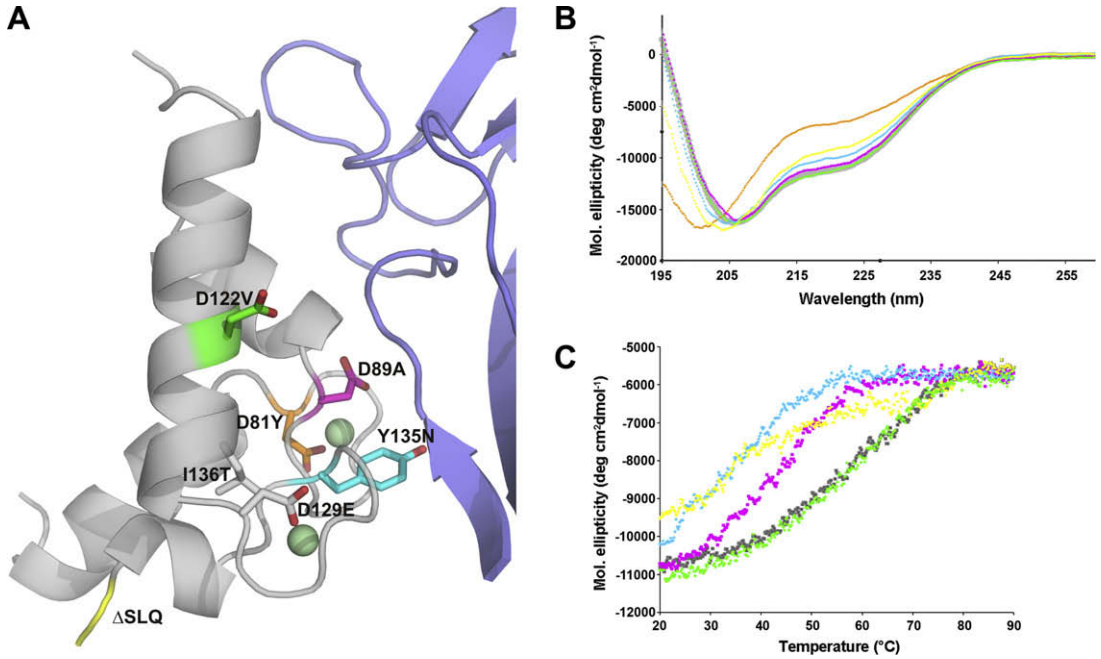

Fig. 2. (A) The interface between MCFD2 (grey) and the CRD (blue) showing the positions of the F5F8D-causing mutations on MCFD2. The positions of the mutations analysed by CD are coloured in orange (D81Y), pink (D89A), green (D122V), cyan (Y135N) and yellow (ΔSLQ). Mutations previously analysed in grey (D129E and I136T). (B) Far-UV CD spectra of MCFD2 and F5F8D mutant variants. Mutant data are shown with the same colour coding as in (A), folded wild type in grey. (C) Thermal unfolding experiments performed monitoring the CD signal at 222 nm. Mutant data are shown with the same colour coding as in (A), folded wild type in grey.

hydrophobic core. CD measurements on the two disease-causing mutations D81Y and D89A in the first Ca^{2+} binding loop indicate that both affect the stability of MCFD2. The spectrum of D81Y has a profile similar to that of the disordered apo state of wild-type MCFD2 [7], indicating that this mutant has lost the ability to bind Ca^{2+} and is disordered. The spectrum of D89A (Fig. 2) resembles that of the Ca^{2+} bound form of wild-type MCFD2 with contribution from α-helical structure with minima at 207 and 222 nm and a change of sign from negative to positive CD at 197 nm. However, the Tm of 43 °C is significantly lower than the 59 °C for wild-type MCFD2. Another patient mutation, Y135N [17] in the second Ca^{2+} binding loop, shows a spectrum indicating a lower α-helical content, albeit not completely disordered, and a Tm of 34 °C. A nonsense mutation causing deletion of the last three amino acids of MCFD2 (ΔSLQ) results in a similar spectral profile, consistent with previous data [16] and due to very low stability a Tm could not be determined. In contrast, the mutant D122V, positioned in the third α-helix, has a spectrum and Tm value identical to wild-type MCFD2. Thus, this mutation does not have a significant structural effect on MCFD2.

4. Discussion

LMAN1 and MCFD2 are present primarily in complex with each other with a 1:1 stoichiometry in vivo [5]. The binding constant for CRD and MCFD2 is 1.6×10^8 M [6] and for CRD and N-terminal truncated MCFD2 in the same order (unpublished data) so the limited 850 $Å^2$ surface area buried upon complex formation is surprising. The binding of MCFD2 does not induce any major structural changes in the CRD and thus it most probably acts as co-receptor in the transport of FV and FVIII by direct interaction with cargo rather than through modulation of the binding of cargo to the CRD. This is consistent with data showing that MCFD2 bearing the D129E mutation, which disrupts the LMAN1–MCFD2 interaction, can still be cross-linked to FVIII [5]. Binding of the cargo in the carbohydrate binding site on the CRD and to the ordered part of MCFD2, requires the cargo to reach over a long stretch on the CRD – more than 45 Å (Fig. 1A). Even if the disordered N-terminal residues and the dynamic loop between the two EF-hands in MCFD2 would constitute the cargo binding residues, the distance to the carbohydrate binding site on the CRD would be of the same order. A perhaps more likely scenario could be that while binding with its sugar moieties to the CRD, the cargo interacts with MCFD2 bound to a neighbouring CRD. LMAN1 assembles into hexamers during cargo transport [9], but in solution the heterodimeric complex of the CRD with MCFD2 shows no signs of oligomerization. Analysis of the packing interactions in the crystal does not reveal any assemblies corresponding to oligomeric receptor complexes. That is not surprising as earlier studies have shown that oligomerization is mediated by the stalk domain [9].

All known *LMAN1* mutations are null alleles except three missense mutations. One of these changes the starting methionine to a threonine and is not translated, while the second, C475R, affects oligomerisation [2]. The third, W67S, which was shown to interfere both with MCFD2 and mannose binding [15], would disrupt the packing of the LMAN1 hydrophobic core, destabilizing the protein. None of these residues are involved in interactions with MCFD2.

Nine of the F5F8D mutations in *MCFD2* disrupt the open reading frame, while the others are substitution mutants. One of these creates a stop codon (ΔSLQ), deleting the last three residues of the protein, which was shown to impede binding to LMAN1 in HeLa cells [16]. Two mutations, D129E and I136T, are located in the second EF-hand motif, and have been shown to abolish the interaction between MCFD2 and LMAN1 in HeLa cells [4]. This was explained by NMR studies which revealed both to be predominantly disordered. F5F8D mutations D81Y, D89A and D122V were shown by co-immunoprecipitation in COS1 cells to abolish MCFD2 binding to LMAN1 [2].

As seen from the CD-data, the MCFD2 mutations D81Y, D129E, I136T, and ΔSLQ all give rise to destabilized proteins which result in F5F8D. D81 and D129 are Ca^{2+} ligands and upon mutation Ca^{2+} can no longer bind, preventing formation of a stable MCFD2. I136

is part of the second Ca^{2+} binding loop and participates in the small hydrophobic core of the protein. Structural disturbance by mutation of this residue would thus both impede Ca^{2+} binding and disturb packing of the hydrophobic core. The instability of the ΔSLQ mutation is more difficult to understand, these residues are disordered in the complex structure, while in the free MCFD2 they interact with the disordered loop between the two EF-hands; the C-terminal carboxyl group forms an ion pair with K102 in the loop. It is possible that this interaction is important for stability of MCFD2 and that the unstructured protein resulting from the mutation is unable to bind to LMAN1. Mutants D89A and Y135N are less severely destabilized but are unable to bind to LMAN1. The side chain of D89 caps the N-terminus of the helix after the first Ca^{2+} binding loop and forms a hydrogen bond to a water ligand of the Ca^{2+} ion. Presumably loss of these interactions gives rise to some destabilization of the D89A mutant as seen in the lowered Tm-value. Furthermore, D89 forms a salt bridge with K53 of the CRD, explaining the loss of LMAN binding [2] and F5F8D for the mutation. The side chain of Y135, which is located in the second Ca^{2+} binding loop, is involved in hydrophobic interactions with L87 and the mutation Y135N can thus cause destabilization of the mutated protein. In addition, in the complex, Y135 packs against F46 in the CRD which would weaken the interaction of Y135N to LMAN1, the combination leading to F5F8D. Finally, the D122V mutant CD-spectra and melting point are indistinguishable from the wild type MCFD2. D122 is located in the middle of helix three and forms a hydrogen bond to Y48 and an ionic interaction with K49 in the CRD. The inability to engage in these interactions severely impedes binding to LMAN1 and results in F5F8D for this mutant.

In conclusion, most of the known F5F8D substitution mutations in MCFD2 cause destabilization of its already inherently flexible structure or loss of interactions with LMAN1. Both mutation effects result in a significantly lower number of competent receptor complexes and inefficient transport of coagulation factors V and VIII from the ER. Interestingly, none of the characterized F5F8D mutations can be implicated in cargo binding.

Acknowledgements

This work was supported by grants from the Human Frontier Science Program and The Swedish Research Council (YL), and The European Commission FP6 Marie Curie programme (IK).

References

[1] Oeri, J. (1954) Congenital factor V deficiency (parahemophilia) with true hemophilia in two brothers. Bibl. Paediatr. 58, 575–588.
[2] Zhang, B., Spreafico, M., Zheng, C., Yang, A., Platzer, P., Callaghan, M.U., Avci, Z., Ozbek, N., Mahlangu, J., Haw, T., Kaufman, R.J., Marchant, K., Tuddenham, E.G.D., Seligsohn, U., Peyvandi, F. and Ginsburg, D. (2008) Genotype-phenotype correlation in combined deficiency of factor V and factor VIII. Blood 111, 5592–5600.
[3] Nichols, W.C., Seligsohn, U., Zivelin, A., Terry, V.H., Hertel, C.E., Weatley, M.A., Moussalli, M., Hauri, H.P., Ciavarella, N., Kaufman, R.J. and Ginsburg, D. (1998) Mutations in the ER–Golgi intermediate compartment protein ERGIC-53 cause combined deficiency of coagulation factors V and VIII. Cell 93, 61–70.
[4] Zhang, B., Cunningham, M.A., Nichols, W.C., Bernat, J.A., Seligsohn, U., Pipe, S.W., McVey, J.H., Shulte-Overberg, U., de Bosch, N.B., Ruiz-Saez, A., White, G.C., Tuddenham, E.G., Kaufman, R.J. and Ginsburg, D. (2003) Bleeding due to disruption of a cargo-specific ER-to-Golgi transport complex. Nat. Genet. 34, 220–225.
[5] Zhang, B., Kaufman, R.J. and Ginsburg, D. (2005) LMAN1 and MCFD2 form a cargo receptor complex and interact with coagulation factor VIII in the early secretory pathway. J. Biol. Chem. 280, 25881–25886.
[6] Kawasaki, N., Ichikawa, Y., Matsuo, I., Totani, K., Matsumoto, N., Ito, Y. and Yamamoto, K. (2008) The sugar-binding ability of ERGIC-53 is enhanced by its interaction with MCFD2. Blood 111, 1972–1979.
[7] Guy, J.E., Wigren, E., Svärd, M., Härd, T. and Lindqvist, Y. (2008) New insights into multiple coagulation factor deficiency from the solution structure of human MCFD2. J. Mol. Biol. 381, 941–955.
[8] Appenzeller, C., Andersson, H., Kappeler, F. and Hauri, H.P. (1999) The lectin ERGIC-53 is a cargo transport receptor for glycoproteins. Nat. Cell Biol. 1, 330–334.
[9] Neve, E.P.A., Lahtinen, U. and Pettersson, R.F. (2005) Oligomerization and intracellular localization of the glycoprotein receptor ERGIC-53 is independent of disulfide bonds. J. Mol. Biol. 354, 556–568.
[10] Appenzeller-Herzog, C. and Hauri, H.P. (2006) The ER–Golgi intermediate compartment (ERGIC): in search of its identity and function. J. Cell Sci. 119, 2173–2183.
[11] Nyfeler, B., Reiterer, V., Wendeler, M.W., Stefan, E., Zhang, B., Michnick, S.W. and Hauri, H.P. (2008) Identification of ERGIC-53 as an intracellular transport receptor of alpha1-antitrypsin. J. Cell Biol. 180, 705–712.
[12] Fraldi, A., Zito, E., Annunziata, F., Lombardi, A., Cozzolino, M., Monti, M., Spampanato, C., Ballabio, A., Pucci, P., Sitia, R. and Cosma, M.P. (2008) Multistep, sequential control of the trafficking and function of the multiple sulfatase deficiency gene product, SUMF1 by PDI, ERGIC-53 and ERp44. Hum. Mol. Genet. 17, 2610–2621.
[13] Velloso, L.M., Svensson, K., Schneider, G., Pettersson, R.F. and Lindqvist, Y. (2002) Crystal structure of the carbohydrate recognition domain of p58/ERGIC-53, a protein involved in glycoprotein export from the endoplasmic reticulum. J. Biol. Chem. 277, 15979–15984.
[14] Velloso, L.M., Svensson, K., Pettersson, R.F. and Lindqvist, Y. (2003) The crystal structure of the carbohydrate-recognition domain of the glycoprotein sorting receptor p58/ERGIC-53 reveals an unpredicted metal-binding site and conformational changes associated with calcium ion binding. J. Mol. Biol. 334, 845–851.
[15] Yamada, T., Fujimori, Y., Suzuki, A., Miyawaki, Y., Takagi, A., Murate, T., Sano, M., Matsushita, T., Saito, H. and Kojima, T. (2009) A novel missense mutation causing abnormal LMAN1 in a Japanese patient with combined deficiency of factor V and factor VIII. Am. J. Hematol. 84, 738–742.
[16] Nyfeler, B., Kamiyaa, Y., Boehlen, F., Yamamoto, K., Kato, K., de Moerloose, P., Hauri, H.P. and Neerman-Arbez, M. (2008) Deletion of 3 residues from the C-terminus of MCFD2 affects binding to ERGIC-53 and causes combined factor V and factor VIII deficiency. Blood 111, 1299–1301.
[17] Ivaskevicius, V., Windyga, J., Baran, B., Bykowska, K., Daugela, L., Watzka, M., Seifried, E. and Oldenburg, J. (2008) The first case of combined coagulation factor V and coagulation factor VIII deficiency in Poland due to a novel p.Tyr135Asn missense mutation in the MCFD2 gene. Blood Coagul. Fibrinolysis 19, 531–534.
[18] Studier, F.W. (2005) Protein production by auto-induction in high density shaking cultures. Protein Expr. Purif. 41, 207–234.
[19] Kabsch, W. (1993) Automatic processing of rotation diffraction data from crystals of initially unknown symmetry and cell constants. J. Appl. Cryst. 26, 795–800.
[20] Collaborative Computational Project, Number 4. (1994). The CCP4 Suite: Programs for Protein Crystallography. Acta Cryst. D 50, 760–763.
[21] McCoy, A.J., Grosse-Kunstleve, R.W., Adams, P.D., Winn, M.D., Storoni, L.C. and Read, R.J. (2007) *Phaser* crystallographic software. J. Appl. Cryst. 40, 658–674.
[22] Cowtan, K. (1994) An automated procedure for phase improvement by density modification. Joint CCP4 and ESF-EACBM Newsletter on Protein Crystallography 31, 34–38.
[23] Emsley, P. Lohkamp, B., Scott W.G. and Cowtan, K. (2010) Features and Development of Coot. Acta Cryst. *D* 66 (in press).
[24] Murshudov, G.N., Vagin, A.A. and Dodson, E.J. (1997) Refinement of macromolecular structures by the maximum-likelihood method. Acta Cryst. D 53, 240–255.
[25] W.L. DeLano, The PyMOL Molecular Graphics System, DeLano Scientific, San Carlos, CA (2002) http://www.pymol.org.